Journal of Colloid and Interface Science **256,** 297–303 (2002)
doi:10.1006/jcis.2002.8691

Synthesis of Gold Nanoparticles in a Winsor II Type Microemulsion and Their Characterization

Abhijit Manna,* Toyoko Imae,*,[1] Toshinobu Yogo,† Keigo Aoi,‡ and Midori Okazaki‡

*Research Center for Materials Science, Nagoya University, Chikusa, Nagoya 464-8602, Japan; †Graduate School of Engineering, Nagoya University, Chikusa, Nagoya 464-8603, Japan; and ‡Graduate School of Bioagricultural Sciences, Nagoya University, Chikusa, Nagoya 464-8601, Japan

Received October 15, 2001; accepted September 4, 2002

Dodecanethiol-capped nanospherical gold metal particles have been synthesized using a biphasic Winsor II type microemulsion of diethyl ether/aerosol-OT/water. The reduction of gold(III) chloride in the presence of dodecanethiol results in the formation of stable, organically soluble nanoparticles of 4 ± 0.6 nm average diameter. The UV–vis plasmon absorption band and transmission electron microscopic (TEM) analysis confirmed the formation and size of the particles. TEM morphology shows a two-dimensional array of these particles with an average spacing between gold cores of about 1.8 nm onto hydrophobic carbon surfaces. Elemental analysis results and the similarity of the Fourier transform infrared (FT-IR) spectrum of free dodecanethiol to that of composite material reveal the encapsulation of gold particles by dodecanethiol. The detailed analysis of FT-IR spectra of our composite material and its comparison with literature reports disclose that a Winsor II type system is superior for the synthesis of nanoparticles bounded by a three-dimensional self-assembled monolayer of alkanethiol with a close-packed *all trans* zigzag conformation. ^{1}H NMR spectroscopic observations suggest the absence of free thiols. X-ray photoelectron spectroscopic analysis supports that the oxidation state of gold is zero (Au^0). Thermogravimetric and differential thermal analysis indicates an interaction between thiol group and gold surfaces and thiol molecule per nearly three gold atoms in the composite particles.

Key Words: **dodecanethiol; Winsor II type microemulsion; gold nanoparticle; UV–vis plasmon absorption band; transmission electron microscopy; X-ray photoelectron spectroscopy; infrared spectroscopy; ^{1}H NMR spectroscopy; thermogravimetric and differential thermal analysis; elemental analysis; two-dimensional array; three-dimensional self-assembled monolayer.**

INTRODUCTION

There is currently much interest in the synthesis of metallic and semiconductive nanoparticles ("quantum dots") in a two-phase medium (1–3). This interest has been fueled by unusual physical properties, which depend on their size, shape, and packing density. For example, while bulk gold is metallic in nature, colloidal gold nanoparticles have electronic properties, which fall somewhere between those of metals and semiconductors. Gold particles have been found to be particularly useful for cell labeling in biology and the formation of a modified surface for surface-enhanced Raman scattering (4).

Brust *et al.* (1) reported a two-phase method using sodium borohydride reduction of an aqueous tetrachloroaurate in excess toluene. Tetraoctylammonium bromide was used as a phase-transfer catalyst to transfer tetrachloroaurate ions from aqueous to organic phase. This is an efficient method for the synthesis of nanoparticles where the transferable metal ion should be anionic in nature. Recently, Sarathy *et al.* (5) developed an acid-facilitated procedure wherein one can transfer the well-characterized nanoparticles from a hydrosol to a nonpolar medium dissolved alkanethiol. However, this procedure has a serious drawback of using excess quantity of concentrated HCl. Our interest lies in the development of two-phase systems for the synthesis of monodispersed nanoparticles, which form an ordered monolayer onto solid surfaces, using common water-soluble salts of noble metals.

Microemulsions are thermodynamically stable dispersions and are divided into four Winsor types, namely, Winsor I, Winsor II, Winsor III, and Winsor IV systems (6, 7). All of these systems maintain a certain microenvironment. The applications of Winsor I (an oil-in-water microemulsion that is in equilibrium with excess oil phase) and Winsor II (a water-in-oil microemulsion that is in equilibrium with excess water phase) type microemulsions in the synthesis of quantum-dot particles are expected to avoid the limitations that may arise due to solubility constraints as discussed above.

Recently, Manna *et al.* (8) reported the synthesis of thiol-capped silver nanoparticles using a Winsor II type microemulsion. They have synthesized silver nanoparticles with an average size of 11 nm with a broad size range of 5 to 17 nm. We report, here, the synthesis of dodecanethiol-capped gold nanoparticles using a Winsor II type microemulsion. This microemulsion system is the two-phase medium in the synthesis of monodispersed organically soluble nanoparticles protected by a three-dimensional self-assembled monolayer (3D-SAM) (9) of highly crystalline alkanethiol. The synthesized particles maintain a precise size range of 2.5 to 5 nm with an average

[1] To whom correspondence should be addressed. Toyoko Imae, Research Center for Materials Science, Nagoya University, Chikusa, Nagoya 464-8602, Japan. Fax: +81-52-789-5912. E-mail: imae@nano.chem.nagoya-u.ac.jp.

0021-9797/02 $35.00

size of 4 ± 0.6 nm. These particles are self-assembled into a two-dimensional (2D) monolayer (10) onto the carbon surfaces.

EXPERIMENTAL

Gold(III) chloride ($AuCl_3$, 99%), sodium bis(2-ethylhexyl) sulfosuccinate (aerosol-OT, AOT, 99%), and sodium borohydride ($NaBH_4$, 99%) were purchased from Aldrich Chemical Co. Ethanol (99.8%) and diethyl ether (99%) were purchased from Wako Chemical Co. Dodecane thiol (extra pure reagent) was a product of Nacalai Tasque, Inc. All these chemicals were used without purification. Milli-Q water was used throughout all experiments.

UV–visible plasma absorption measurement was carried out at room temperature on a Shimadzu UV 2200 UV–vis spectrometer using a quartz cell (10-mm path). A dilute solution of nanoparticles in *n*-heptane was used for this analysis. Backgrounds of the spectra were subtracted by the UV–vis spectra of the same solvent.

Specimen for transmission electron microscopy (TEM) was prepared by spreading a small drop ($\sim 2\ \mu$L) of a dilute *n*-heptane solution onto a standard copper grid coated with a thin amorphous Formvar carbon film and letting the drop dry completely in air. The particle size and morphology were observed at room temperature on a Hitachi H-800 electron microscope operating at 100 kV. The size distribution and standard deviation were derived by measuring the diameter of nearly 200 particles from different parts of the specimen.

A Perkin–Elmer PE 2400 instrument was used for elemental analysis.

Fourier transform infrared (FT-IR) spectra in the region of 3500 to 1000 cm^{-1} were recorded at room temperature on a Bio-Rad FTS 575C FT-IR instrument. The KBr pellets were used as supporting materials for analysis. A drop of free dodecane thiol and a powder specimen were used for recording spectra of free thiol and nanoparticles, respectively.

^{1}NMR spectra were recorded on a Bruker ARX 400 spectrometer operating at 400 MHz. The data were collected using deuterated toluene (C_6D_5–CD_3) as the solvent.

The X-ray photoelectron spectroscopic (XPS) signals were recorded on a JEOL JPS-9000MC spectrometer operated at a base pressure lower than 10^{-7} Pa. The different core level spectra were recorded using Mg$K\alpha$ radiation ($h\nu = 1253.6$ eV) with an X-ray source operated at a power of 10.0 kV and a current of 10.0 mA. The spectra of the C1*s*, S2*p*, and Au4*f* orbitals were recorded at an overall instrumental resolution of $\sim$0.9 eV. The specimen used for this analysis was the dry powder of composite material.

Thermogravimetric and differential thermal analysis (TG/DTA) was performed with a Seiko TG/DTA 6200 instrument. At a heating rate of 10°C/min, the measurement of the specimen was carried out from 30 to 700°C under flowing nitrogen at 200 cm^3/min. To remove adsorbed water, the sample was preheated at 110°C for 30 min.

RESULTS AND DISCUSSION

Preparation of nanoparticles. The two-phase redox reaction was carried out in water/AOT/diethyl ether along with the dodecanethiol system by using redox reagents soluble in the adjoining phase. We have preferred AOT as the surfactant due to its higher solubility in organic phase and its anionic character, which helps to extract metal cations from the aqueous to reverse micellar phase. The extracted gold ions were reduced with aqueous sodium borohydride, following the redox reaction:

$$2AuCl_3 + 6NaBH_4 + 18H_2O = 2Au + 6NaCl + 6H_3BO_3 + 21H_2$$

Ten cubic centimeters of aqueous 0.02 M $AuCl_3$ solution and 40 cm^3 of a 0.05 M AOT solution in diethyl ether were mixed together and stirred vigorously for 1 h. Subsequently, it was allowed to separate into two distinct transparent phases, resulting in a quantitative transfer of Au^{III} ions from an aqueous to reverse microemulsion (diethyl ether) phase. Forty-five milligrams (2.2×10^{-4} mol) of dodecanethiol was then added to the rapidly stirring microemulsion for a few minutes. After that, 10 cm^3 of an aqueous 0.2 M $NaBH_4$ solution (freshly prepared) was slowly added to the mixture with vigorous stirring; stirring was continued for 2 h to complete the reaction, followed by two-phase separations. The wine-red reverse micellar phase containing a large quantity of precipitates was in equilibrium with a clear aqueous phase; the reverse micellar phase was separated and evaporated to dryness at 50°C in atmospheric conditions. The crude product was suspended in 25 cm^3 of ethanol and solid was extracted by filtration of the ethanol solution through 0.2-μm Millipore filter paper under pressure. The solid was thoroughly washed with excess ethanol to eliminate unreacted thiol and AOT adsorbed on the surface of the particles. The purified solid was dried at 50°C. Yield was 55% with respect to the total weight of Au and thiol used.

The dry waxy powder obtained was soluble in nonpolar organic solvents like *n*-pentane, *n*-hexane, *n*-heptane, and toluene. The colloidal solution of the particles in heptane was stable for more than several months.

Characterization of nanoparticles. The UV–vis absorption spectra (Fig. 1) in heptane solution show an absorption band with a peak maximum at 525 nm. The gold particles are known to have an intense plasmon absorption band in this region (10, 11). Thus, the absorption band at 525 nm arises from surface plasmon absorption of gold cluster.

Figure 2a shows the bright field TEM photograph of the thiol-stabilized nanoparticles. The photograph shows that all the particles are spherical. The particle distribution, Fig. 2b, shows that all particles are within the 2.5- to 5-nm size range. The photograph also shows that particles are not agglomerated during the evaporation of *n*-heptane in a dispersion of size-monodispersed dodecanethiol-capped gold nanocrystals on a carbon substrate. These nanocrystals yield a monolayer consisting of a

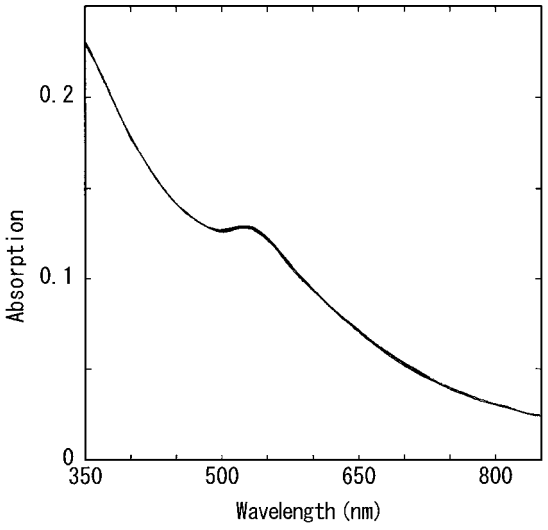

FIG. 1. UV–vis absorption spectrum of dodecanethiol-protected gold nanoparticles in *n*-heptane solution.

2D hexagonal array with some defect. The chemisorbed long-chain dodecanethiol molecules maintain a separation between gold cores after solvent removal with a characteristic interparticle spacing or effective soft sphere radius (12a). The mean diameter and average spacing between metal cores of the particles are 4.0 ± 0.6 nm and 1.8 nm, respectively.

AOT has dual roles, i.e., the formation of microenvironments and the extraction of metal ions from aqueous to organic phase. On the other hand, the strong interactions between Au^0 and SH groups help to form a "three-dimensional self-assembled monolayer" (3D-SAM) (9) onto the particle surfaces. Thus, the dual role of AOT and the interaction between SH groups and gold-particle surfaces control the growth and stabilization of nanocrystals.

The narrow size distribution allows the particles to order into a 2D hexagonal close-packed array. The average spacing (1.8 nm) between metal cores is nearly equal to the single-chain length of dodecanethiol. This intercore spacing is comparable to the results reported by Motte and Pileni (12b). This behavior can be explained by considering the chain conformation. The dodecanethiol molecule forms a densely packed 3D-SAM onto the nanocrystal surfaces. The adjacent particle separation of only one chain length suggests that the ordering arises from the tilt of alkyl chains on a particle. These results indicate the following important information. (i) The sample prepared in this work is monodispersed gold nanoparticles with a narrow size distribution. (ii) The particles are self-assembled into a 2D monolayer (10) onto the hydrophobic carbon surfaces. (iii) During 2D-monolayer formation of particles, alkyl chains of dodecanethiols tilt on gold particles.

A comparison of the particle sizes between Au and Ag particles reveals that the gold particles are nearly 3 times smaller (∼4 nm) than the silver particles (∼11 nm) synthesized under similar conditions (8). This size difference can be explained as follows. The standard redox potentials of Au^{3+}/Au ($E_{Au^{3+}/Au}$) and Ag^{+}/Ag ($E_{Ag^{+}/Ag}$) are 1.002 and 0.79 V, respectively (13). The higher potential of the Au^{3+}/Au pair (compared with the Ag^{+}/Ag system) favors the faster rate of reduction, resulting in the formation of smaller metal particles. The other possibility for the formation of smaller gold particles is the lower reactivity of the gold (Au^0) than silver (Ag^0) (14). The lower reactivity of the gold clusters results in the formation of smaller nanoparticles compared to that of the silver.

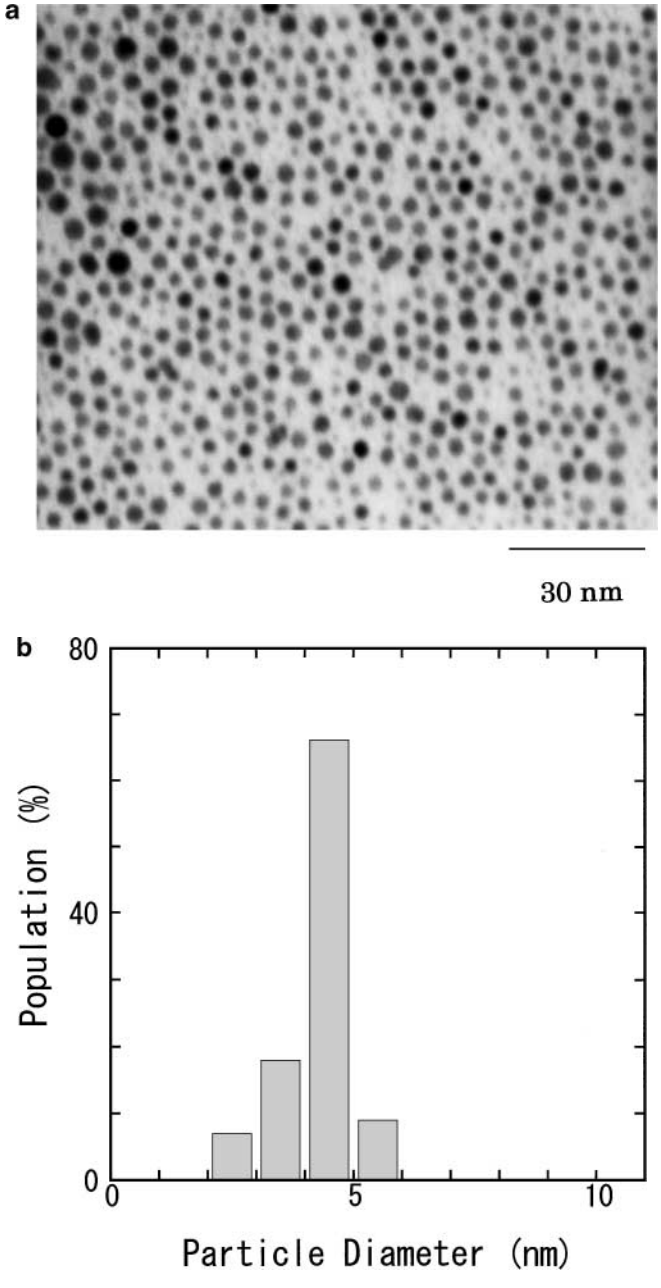

FIG. 2. (a) TEM micrograph of dodecanethiol-protected gold nanoparticles deposited on a carbon surface and (b) size distribution of ∼200 particles.

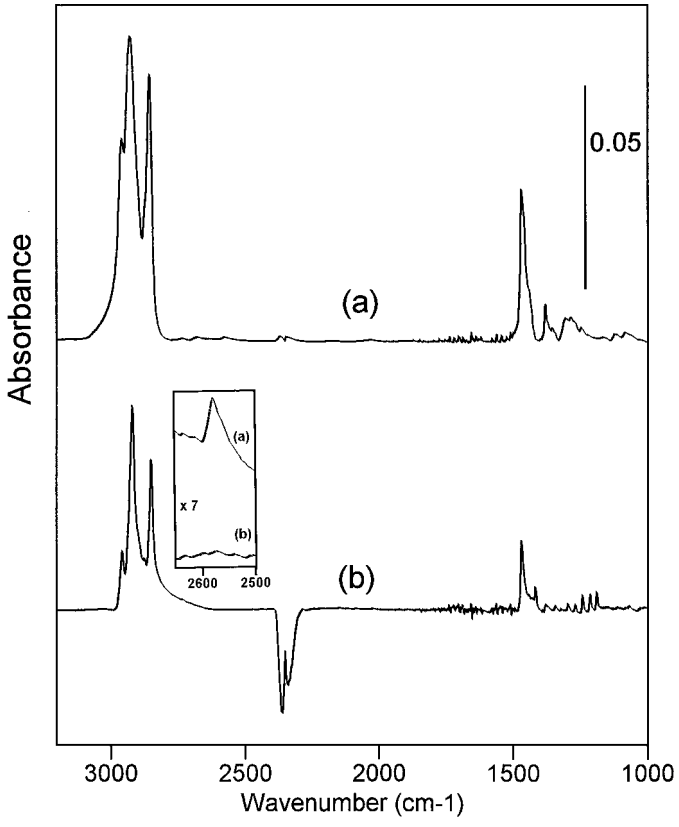

FIG. 3. FT-IR spectra of (a) free dodecanethiol and (b) dodecanethiol-protected gold nanoparticles at 3100–1000 cm^{-1}. The spectra, (a) and (b), shown in the insert are multiplied by a factor of 7 to increase the SH band intensity.

Elemental analysis of the thiol-protected nanoparticle for C, H, and S is 18.48, 3.17, and 4.11 wt%, respectively. The total organic content is ~25 wt%. The atomic percentage of C, H, and S, are respectively as follows: found in our nanocomposite 71.73, 12.30, and 15.97 wt% and calculated 71.57, 12.51, and 15.92 wt%. The atomic percentages of C, H, and S found in the elemental analysis are all in close agreement with the composition of the dodecanethiol, which supports its adsorption on the nanoparticle surface.

FT-IR spectra of the free dodecanethiol and the composite material are shown in Fig. 3. The main bands in these spectra are clearly seen (9, 15–21). The similarity of the features of FT-IR spectra confirms (a) that the thiol is an essential component of the composite nanoparticles and (b) that the thiol molecule is not leached out during several washings of the solid.

The peak positions and vibrational assignments are summarized in Table 1. The fact that the CH_2 antisymmetric and symmetric stretching bands are observed at 2918 and 2848 cm^{-1} in a spectrum of nanoparticles (Fig. 3b) suggests that the alkyl chains of dodecanethiol are extended with a trans zigzag conformation onto the gold particle surface (17, 19). The higher wavenumbers of CH_2 stretching modes observed at 2927 and 2855 cm^{-1} for free dodecanethiol (Fig. 3a) have to be attributed to a greater proportion of gauche conformations (9). By the way, the peak positions of CH_3 asymmetric and symmetric stretching vibration modes at ~2956 and ~2873 cm^{-1} are nearly invariant with respect to the 3D-SAM formation onto the particle surfaces. A similar invariant was found even for CH_2 scissoring (1467 cm^{-1}) and CH_3 symmetric bending (~1377 cm^{-1}) bands (9).

The very weak SH stretching vibration mode is usually observed at ~2560 cm^{-1} (14, 16). The SH stretching vibration band of free dodecanethiol was found at 2575 cm^{-1} in Fig. 3a. However, its absorbance disappeared or was extremely weakened in the composite material (Fig. 3b), as compared in an inserted figure in Fig. 3. These results indicate the disruption of a SH bond and the formation of a Au–S bond. In the spectrum of a dodecanethiol-stabilized gold nanoparticle, Fig. 3b, a new band appearing at 1415 cm^{-1} can be assigned to a scissoring vibration mode of the methylene group adjacent to the Au–S bond. Our result is consistent with those reported by others (9, 21). Thus, the appearance of this band also confirms the formation of a Au–S bond.

The FT-IR spectrum of free dodecanethiol in Fig. 3a shows a weak band at 1302 cm^{-1} corresponding to the gauche conformation (9). The disappearance of this band in the composite material (Fig. 3b) indicates the absence of the gauche conformation (in the alkanethiol chain) in the 3D-SAM system. These results are in agreement with the fact observed in the CH_2 stretching region.

In addition, the formation of order conformation with preferential *all trans* characteristic of an alkanethiol chain was evidenced by sharp changes in the spectral pattern between 1300 and 1150 cm^{-1}, where twisting, rocking, and wagging bands appear (3). For example, the bands at 1281, 1270, and 1245 cm^{-1} are weak and very broad in the spectrum of free dodecanethiol

TABLE 1
FTIR Data for Free Dodecanethiol and Thiol-Capped Gold Nanoparticle (in cm^{-1})

Assignment	Free dodecanethiol	Nanoparticle
CH_3 asymmetric stretching	2957 (m)	2955 (m)
CH_2 antisymmetric stretching	2927 (vs)	2918 (vs)
Fermi resonance	2898 (sh)	2894 (sh)
CH_3 symmetric stretching	2874 (sh)	2873 (w)
CH_2 symmetric stretching	2855 (vs)	2848 (vs)
SH stretching	2575 (vw)	—
CH_2 scissoring	1467 (s)	1467 (s)
CH_2 scissoring adjacent to the Au–S bond	—	1415 (m)
CH_3 symmetric bending (umbrella type)	1378 (m)	1377 (w)
CH_2 twisting, rocking, and wagging	1302 (w)	—
CH_2 twisting, rocking, and wagging	1281 (w)	1294 (w)
CH_2 twisting, rocking, and wagging	1270 (w)	1267 (w)
CH_2 twisting, rocking, and wagging	1245 (vw)	1240 (m)
CH_2 twisting, rocking, and wagging	—	1212 (m)
CH_2 twisting, rocking, and wagging	—	1187 (m)

Note. Very strong (vs), strong (s), medium (m), weak (w), very weak (vw), and shoulder (sh).

(Fig. 3a), whereas very sharp features are seen for the bands at 1294, 1267, and 1240 cm^{-1} in the spectrum of composite materials, Fig. 3b. In addition to these bands, two new bands were found at 1212 and 1187 cm^{-1} due to 3D-SAM formation on a gold surface. The sharp features in this region confirm the crystalline phase of dodecanethiol (3, 9, 18).

It is important to report here that the FT-IR spectral feature of our sample is very similar to that by Kang and Kim (3). They prepared dodecanethiol-passivated silver nanoparticles in one-phase and two-phase systems and compared the crystallinity of alkanethiol chains. They found that the crystallinity of the alkanethiol is excellent for nanoparticle synthesis in a one-phase system, whereas particle synthesis in a two-phase system shows poor crystallinity. Finally, they claimed that the one-phase system is very effective (compared to the two-phase system) in the synthesis of nanoparticles bound by the highly ordered alkanethiol. We have synthesized nanoparticles protected by highly ordered dodecanethiol in a Winsor II system. Thus, the two-phase system reported here is also effective for the synthesis of nanoparticles passivated by alkanethiol with a close-packed *all trans* zigzag conformation.

^{1}H NMR spectroscopic data are very useful in the characterization of thiol molecules bound and unbound to the SAM. Here, we have used these data to characterize the thiol molecules of the nanocomposite. The spectra (not shown) obtained in $C_6D_5CD_3$ reveal two resonances at δ0.8–0.9 (for H of CH_3 group) and 1.1–1.6 (for H of C_β) ppm. The resonance at δ2.2–2.5 ppm that corresponds to H atoms bound to the C_α in free alkanethiol (22) was undetected. These observations suggest that all thiol molecules are attached to the surface of the nanoparticle via the sulfur atom.

High-resolution XPS spectra are shown in Fig. 4. The spectra indicate the presence of both the Au (Fig. 4a) and the alkanethiol (Fig. 4b) in a composite material. The spectrum of the Au4f band serves two gold bands, namely, $4f_{7/2}$ and $4f_{5/2}$, which are identified at 83.8 and 87.5 eV, respectively, as listed in Table 2. The positions and the difference between two peaks (3.7 eV) observed here are exactly the same values as those reported in the literature for the zero valence gold (1). The absence of a Au(III) ion peak at 84.9 eV also indicates that the gold atoms in nanoparticles are present largely as Au^0 (23a). The S2p spectrum gave a weak signal due to the small scattering cross section of the S and the lower amount of material present. The signal consists of a doublet, S2$p_{3/2}$ and S2$p_{1/2}$, at 162.2 and 163.2 eV, respectively (Table 2). The C1s region contains a band at 284.6 eV. This band corresponds to C–C bond atoms and is compared well with a characteristic peak at 284.5 eV reported in the literature (23, 24). The spectra for the S and C regions are very consistent with the spectra of the alkanethiol SAM on gold (23). These results confirm that the composite material consists of Au^0 and dodecanethiol.

Figure 5 represents TG/DTA of the gold nanoparticles. The TGA curve shows a sharp weight loss in the range 260–285°C. This weight loss corresponds to the loss of the dodecanethiol molecules. The weight loss in this range is supported by a peak

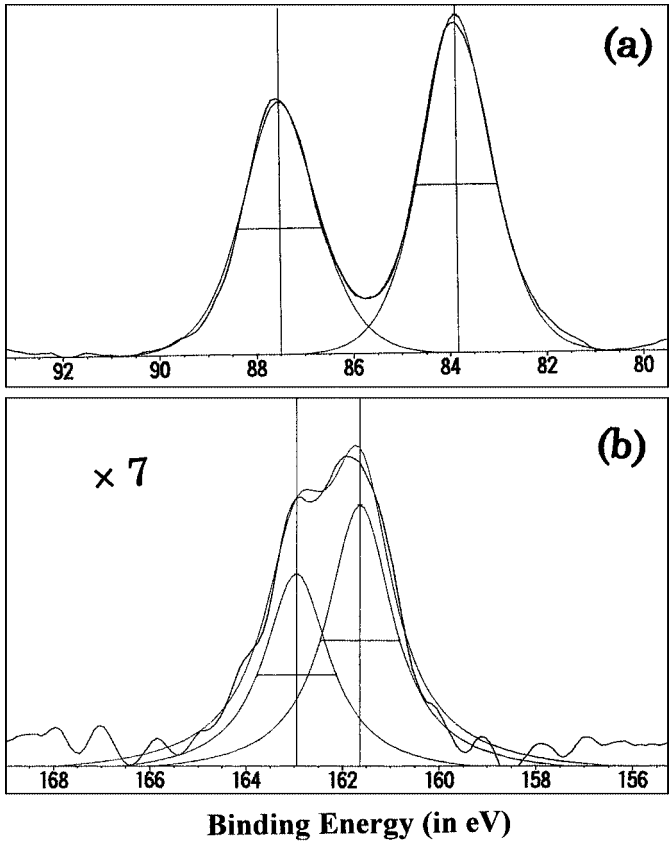

FIG. 4. High-resolution XPS spectra of the powder specimen of the dodecanethiol-protected gold nanoparticles: (a) Au4f and (b) S2p.

of the DTG profile (with a maximum rate of weight loss of 8.4 wt%/min at 281°C). The total TG weight loss of the particles in the above temperature range was ~24 wt%, which is in good agreement with the result of the elemental analysis. There was a negligible change between the temperatures of 300–700°C, probably due to the formation of metallic gold (~76 wt%). These wt% results indicate that the ratio of thiol molecule to gold atom of 4-nm-sized gold particles is about 1/3. The DTA profile shows two endothermic and one exothermic peaks. The endothermic peak observed at ~130°C is probably a result of the reorganization of dodecanethiol chains onto the surface of

TABLE 2
Binding Energy of Elements Obtained from XPS Analysis

	Gold, $4f_{7/2\&5/2}$	Sulfur, $2p_{3/2\&1/2}$	Carbon, 1s
Dodecanethiol SAM,[a] $C_{12}H_{26}S$	—	~162 and ~163 eV	284.5 eV
Metallic gold[b]	~83 and ~87 eV	—	
Nanoparticle in present work	83.8 and 87.5 eV	162.2 and 163.2 eV	284.6 eV

[a] Reference 23.
[b] Reference 1.

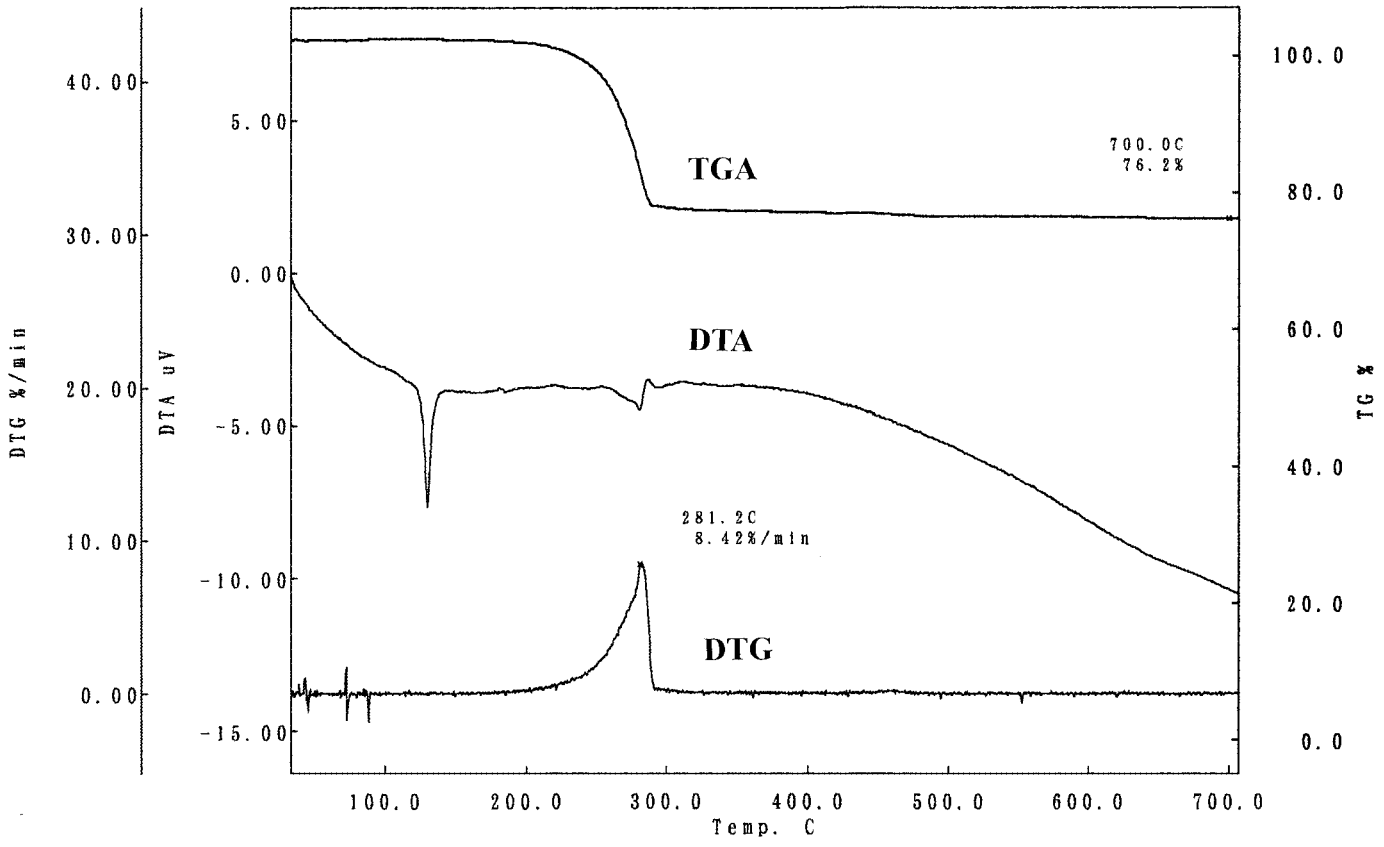

FIG. 5. TG/DTA for dodecanethiol-protected gold nanoparticles.

the Au nanoparticle. The broad and weak endothermic peak at ~285°C supports the cutting off of the Au^0–S bonds and desorption of the dodecanethiol molecules, which is consistent with the support of the loss of dodecanethiol molecules from the TGA curve. The very broad exothermic curve covering a large range (300–600°C) may be due to the large decomposition range of thiol molecules. Thus, TG/DTA results also support the interaction between the thiol group and gold surface and thiol molecule per nearly three gold atoms in the composite nanoparticle.

CONCLUSIONS

The synthesis of stable alkanethiol-passivated nanoparticles using a Winsor II type microemulsion has advantages over conventional two-phase methods. For example, (i) the AOT has dual roles in the formation of a microemulsion and the transfer of charged metal ions from aqueous to organic phase. (ii) The composite nanoparticle behaves like a simple chemical compound, solves in a nonpolar solvent, and forms a hexagonal 2D array onto a hydrophobic carbon surface. (iii) The Winsor II type system is an available one for the synthesis of nanoparticles bound by a 3D-SAM of alkanethiol with a close-packed *all trans* zigzag conformation. These particles are promising for several applications including the manufacturing of optical gratings, optical filters, selective solar absorbers, data storage, and microelectronic devices (25, 26).

REFERENCES

1. Brust, M., Walker, M., Bethell, D., Schiffrin, D. J., and Whyman, R., *J. Chem. Soc. Chem. Commun.* **801** (1994).
2. Heath, J. R., Knobler, C. M., and Leff, D. V., *J. Phys. Chem. B* **101,** 189 (1997).
3. Kang, S. Y., and Kim, K., *Langmuir* **14,** 226 (1998).
4. (a) Freeman, R. G., Grabar, K. C., Allison, K. J., Bright, R. M., Davis, J. A., Guthrie, A. P., Hommer, M. B., Jackson, M. A., Smith, P. C., Walter, D. G., and Natan, M. J., *Science* **267,** 1629 (1995). (b) Johnson, S. R., Evans, S. D., Mahon, S. W., and Ulman, A., *Langmuir* **13,** 51 (1997).
5. Sarathy, K. V., Kulkarni, G. U., and Rao, C. N. R., *J. Chem. Soc. Chem. Commun.* **537** (1997).
6. Lattes, A., Rico, I., de Savignac, A., and Samii, A., *Tetrahedron* **43,** 1725 (1987).
7. Gan, L. M., and Chew, C. H., *Bull. Singapur Natl. Inst. Chem.* **23,** 27 (1995).
8. Manna, A., Kulkarni, B. D., Bondoypadhayay, K., and Vijayamohanan, K., *Chem. Mater.* **9,** 3032 (1997).
9. Hostetler, J. M., Stokes, J. J., and Murray, R. W., *Langmuir* **12,** 3604 (1996).
10. Taleb, A., Petit, C., and Pileni, M. P., *J. Phys. Chem. B* **102,** 2214 (1998).
11. Henglein, A., *Langmuir* **15,** 6738 (1999).
12. (a) Korgel, B. A., Fullam, S., Connonlly, S., and Fitzmaurice, D., *J. Phys. Chem. B* **102,** 8379 (1998). (b) Motte, L., and Pileni, M. P., *J. Phys. Chem. B* **102,** 4104 (1998).

13. Emsley, J., *in* "The elements," 3rd ed., pp. 87, 192. Clarendon, Oxford, 1998.
14. Laibinis, P. E., Whitesides, G. M., Allara, D. L., Tao, Y.-T., Parikh, A. N., and Nuzzo, R. G., *J. Am. Chem. Soc.* **113,** 7152 (1991).
15. (a) Silverstein, R. M., and Bassler, G. C., "Spectrometric Identification of Organic Compounds." Wiley, New York, 1963. (b) Ulman, A., "An Introduction of Ultrathin Organic Films." Academic Press, San Diego, 1991.
16. Hayashi, M., Shiro, Y., and Murata, H., *Bull. Chem. Soc. Jpn.* **39,** 112 (1966).
17. Proter, M. D., Bright, T. B., Allara, D. L., and Chidsey, C. E. D., *J. Am. Chem. Soc.* **109,** 3559 (1987).
18. Bain, C. D., Troughton, E. B., Tao, Y.-T., Whitesides, G. M., and Nuzzo, R. G., *J. Am. Chem. Soc.* **111,** 321 (1989).
19. Nuzzo, R. G., Dubois, L. H., and Allara, D. L., *J. Am. Chem. Soc.* **112,** 558 (1990).
20. Weers, J. G., and Scheuing, D. R., *in* "Fourier Transform Infrared Spectroscopy in Colloid and Interface Science" (D. R. Scheuing, Ed.), ACS Symposium Series 447, p. 87. Am. Chem. Soc., Washington, DC, 1991.
21. Smith, E. L., and Porter, M. D., *J. Phys. Chem.* **97,** 8032 (1993).
22. (a) Ingram, R. S., Hostetler, M. J., and Murray, R. W., *J. Am. Chem. Soc.* **119,** 9175 (1997). (b) Porter, L. A., Jr., Ji, D., Westcott, S. L., Graupe, M., Czernuzewicz, R. S., Halas, N. J., and Lee, T. R., *Langmuir* **14,** 7378 (1998).
23. (a) McNeillie, A., Brown, D. H., Smith, W. E., Gibson, M., and Watson, L., *J. Chem. Soc., Dalton Trans.* **767** (1980). (b) Evan, S. D., Goppert-Berarducci, K. E., Urankar, E., Gerenser, L. J., Ulman, A., and Snyder, R. G., *Langmuir* **7,** 2700 (1991). (c) Barr, T. L., "Modern ESCA: The Principles and Pratice of X-ray Photoelectron Spectroscopy." CRC Press, Boca Raton, FL, 1994.
24. Kumar, A., and Whitesides, G. M., *Science* **263,** 60 (1994).
25. Hahn, R. E., and Seraphin, B. O., "Physics of Thin Film." Academic Press, New York, 1978.
26. (a) Brast, M., Bethell, D., Schiffrin, D. J., and Kiely, C., *Adv. Mater.* **7,** 795 (1995). (b) Collier, C. P., Saykally, R. J., Henrichs, S. E., and Heath, J. R., *Science* **277,** 1978 (1997).